

available at [www.sciencedirect.com](http://www.sciencedirect.com)[www.elsevier.com/locate/brainres](http://www.elsevier.com/locate/brainres)
**BRAIN  
RESEARCH**

## Research Report

# Hemoglobin crystals: A pro-inflammatory potential confounder of rat experimental intracerebral hemorrhage

Timothy J. Kleinig<sup>a,b,\*</sup>, Stephen C. Helps<sup>a,b</sup>, Mounir N. Ghabriel<sup>c</sup>, Jim Manavis<sup>b</sup>, Christopher Leigh<sup>c</sup>, Peter C. Blumbergs<sup>a,b</sup>, Robert Vink<sup>a,b</sup>

<sup>a</sup>Discipline of Pathology, University of Adelaide, Adelaide, SA, Australia

<sup>b</sup>Centre for Neurological Diseases, Hanson Institute, Adelaide, SA, Australia

<sup>c</sup>Discipline of Anatomical Sciences, University of Adelaide, Adelaide, SA, Australia

### ARTICLE INFO

#### Article history:

Accepted 24 June 2009

Available online 1 July 2009

#### Keywords:

Hemoglobin

Inflammation

Intracerebral hemorrhage

### ABSTRACT

In vivo rat hemoglobin crystallization has been reported in lung, liver and kidney, but never following central nervous system injury. In the present study, we examined hemoglobin crystallization following experimental intracerebral hemorrhage (ICH) and its effects on inflammation. Ninety-one rat brains, subjected to either autologous or collagenase ICH, and vehicle controls, were retrospectively examined. In both models, hemoglobin crystals were present in most brains at 24 and 48 h. They were especially prominent at 24 h in autologous ICH brains (2.5% of the hematoma vs 0.6% in collagenase animals;  $p=0.0001$ ) and, at 5 h, were only present in autologous ICH brains. Crystals were diminishing at 48 h and were absent at 7 days. Crystals appeared in clusters around blood vessels. In both models, at 24 h, crystals appeared strongly chemotactic for neutrophils. This effect was most pronounced in autologous ICH brains ( $2628 \pm 182$  neutrophils/mm<sup>2</sup> hematoma crystals vs  $327 \pm 54$  neutrophils/mm<sup>2</sup> hematoma;  $p < 0.0001$ ). In these animals up to 30% of the total neutrophilic infiltrate was located around crystals. A greater overall neutrophilic infiltrate was seen in autologous ICHs with higher percentages of crystalline hemoglobin ( $p=0.04$  for trend). Although hemoglobin crystallization occurs in both models of ICH, it is particularly prominent following autologous ICH. Accordingly, hemoglobin crystallization may exaggerate the importance of inflammation in this model.

© 2009 Elsevier B.V. All rights reserved.

## 1. Introduction

Animal models of intracerebral hemorrhage (ICH) imperfectly mimic human disease (James et al., 2008). The most widely-used models are autologous blood (Whisnant et al., 1963) or collagenase injections (Rosenberg et al., 1990) into the brains of mice or rats (James et al., 2008). The pathological responses to these two models ICH differ significantly (MacLellan et al., 2008). Additionally, the pathophysiology of both of these models is known to differ in several ways from human ICH (for

instance, the tempo of edema formation (Xi et al., 2006) and hematoma resorption (MacLellan et al., 2008)).

In this report we demonstrate a further difference, both between models and between rodent and human ICH: the presence of hemoglobin crystallization, which appears to evoke an exaggerated inflammatory response.

Whereas hemoglobin from humans and most other species crystallizes in vivo only if structurally abnormal, it has been known for some decades that rat hemoglobin readily crystallizes in vitro (Squires and McFadzean, 1963) and may even exist

\* Corresponding author. Discipline of Pathology, University of Adelaide, SA, Australia, 5005. Fax: +61 8 8222 3093.

E-mail address: [timothy.kleinig@adelaide.edu.au](mailto:timothy.kleinig@adelaide.edu.au) (T.J. Kleinig).

Abbreviations: ICH, Intracerebral hemorrhage; EM, Electron microscopy; H and E, Hematoxylin and eosin; DAB, Diaminobenzidine

in a partially crystalline state within erythrocytes (Brunori et al., 1982). In vivo rat hemoglobin crystallization was first noted incidentally after toxin injury to lung (Harris and Chen, 1970), and characterized more completely following injury (graded pressure) to dentition (Rygh and Selvig, 1973). In this setting, hemoglobin crystals were noted after only 2 h of pressure; they became increasingly prominent by 24 h, but were absent at 60 h. The authors concluded that they represented an intermediate state of rat hemoglobin break-down. There have been several subsequent reports of hemoglobin crystallization following injury of varying etiologies to rat lung (Ghio et al., 2000; Paakko et al., 1996; Zachary et al., 2001) and kidney (Madsen et al., 1982), but never following central nervous system injury. In these studies hemoglobin crystals have been deemed a curiosity without pathophysiological significance. In the current study we show that hemoglobin crystallization occurs in rats following both autologous and collagenase ICH, and is particularly prominent following autologous ICH. Furthermore, we demonstrate that hemoglobin crystallization appears to exaggerate the ICH-induced inflammatory response.

## 2. Results

### 2.1. Time-course and appearance of crystals in relation to hematoma

At early timepoints H and E stained sections through the hematoma centre demonstrated crystalline structures (Figs. 1a, b). At 5, 24 and 48 h a greater percentage of the hematoma area

was occupied by crystalline structures in the autologous ICH group than in the collagenase group (Table 1). In both models crystals were most prominent at the 24 hour timepoint (Table 1). Crystals were evident at 5 h in 4/5 autologous ICH animals (but not in 5 collagenase ICH animals). At 24 h they were present in 5/5 autologous ICH animals and 13/15 collagenase ICH animals and at 48 h in 4/5 autologous and 3/5 collagenase ICH animals. Crystals in both groups appeared to be disintegrating by 48 h (Figs. 1c, d) and no crystals were visible by 7 days in either group (Table 1), in rough parallel with hematoma resorption (Fig. 2a).

Crystals were tetragonal in shape and ranged from 0.5 to 20  $\mu\text{m}$  in width and up to 166  $\mu\text{m}$  in length. Crystals were commonly clustered around blood vessels (Fig. 1a), were eosinophilic, and, like rat erythrocytes, were sometimes pitted.

0.2 U of bacterial collagenase has previously been reported to cause a similar hematoma volume to 100  $\mu\text{L}$  autologous blood (MacLellan et al., 2008), however final autologous ICH hematoma volumes were around 30% smaller in our experiments (Fig. 2a). This did not appear to influence crystal formation, however, as, in the collagenase group, which has an inherent variability of hematoma size (as blood is not directly injected) there was no correlation between hematoma size and the percentage of the hematoma occupied by crystals (Fig. 2b).

### 2.2. Identification of crystals

Under light microscopy, microscopy eosinophilic staining of crystals appeared identical to adjacent erythrocytes. This characteristic, as well as a 'pitted' appearance, has previously

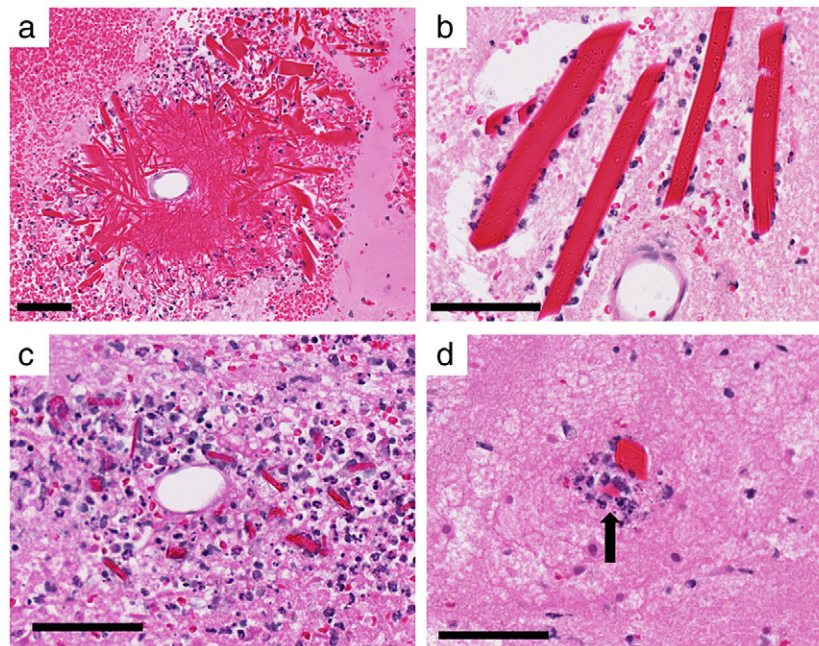


**Fig. 1 – Staining of crystals following rat ICH. Scale bar 100  $\mu\text{m}$ . (a) H and E, rat striatum, autologous ICH, 24 h. A large perivascular crystal cluster between areas of intact and lysed erythrocytes. Most visible neutrophils are closely associated with crystals; (b) H and E, rat striatum, collagenase ICH, 24 h. Large crystals amongst ghost erythrocytes, surrounded by palisading neutrophils; (c) H and E, rat striatum, autologous ICH, 48 h. A perivascular cluster of disintegrating crystals, surrounded by leucocytoclastic nuclear debris; (d) H and E, rat striatum, collagenase ICH, 48 h. A disintegrating crystal (arrow) adjacent to a better preserved crystal, both surrounded by leucocytes.**

**Table 1 – Percentages of hematoma centre area occupied by crystals and percentage of total ipsilateral inflammatory cell infiltrate associated with crystals at all timepoints (peak (24 in bold)).**

	% Hematoma occupied by crystals	% Neutrophils peri-crystalline	% Activated microglia peri-crystalline
5 h autologous ICH	1.3% (0–5.1)*	0	0
5 h collagenase ICH	0%	N/A	N/A
<b>24 h autologous ICH</b>	<b>2.5% (1.4–3.7)***</b>	<b>22.1% (15.4–30.2)***</b>	<b>8.3% (5.7–12.8)***</b>
<b>24 h collagenase ICH</b>	<b>0.6% (0–1.7)</b>	<b>3.3% (0–14.9)</b>	<b>1.5% (0–6.7)</b>
48 h autologous ICH	0.3% (0–0.6%)	0.9% (0–2.6%)	2.2% (0–4.6%)
48 h collagenase ICH	0.04% (0–0.2%)	0.4% (0–2.0%)	0.2% (0–0.6%)
7 day autologous ICH	0%	N/A	N/A
7 day collagenase ICH	0%	N/A	N/A

Figures in brackets represent the range \* $p < 0.05$ , \*\*\* $p < 0.001$  (comparisons between autologous and collagenase groups at equivalent timepoints). Crystals comprised a greater percentage of the hematoma in autologous ICH animals at all timepoints. Crystal formation peaked in both models at 24 h (bold type). In the autologous model, peri-crystalline (within 50  $\mu\text{m}$  of crystals) infiltrating inflammatory cells comprised a significant percentage of total inflammatory cell infiltrate.

been noted in rat hemoglobin crystals. These ‘pits’ have been shown to be lamellar inclusion bodies and are present in both rat hemoglobin crystals and erythrocytes (Paakko et al., 1996).

DAB staining demonstrated confluent brown staining of crystals, adjacent red blood cells and, to a lesser extent, areas of erythrocyte lysis (Fig. 3a), indicating that both crystals and erythrocytes possessed endogenous peroxidase activity (in erythrocytes this is conferred by the heme group). No other

DAB staining was seen in the rest of the brain. Modified Lillie’s stain at 24 h for ferrous iron demonstrated blue staining of both erythrocytes and crystals (Figs. 3b, c). Lillie’s stain for ferric iron (the oxidized state following conversion by heme oxygenase) at this time point was negative (data not shown). Crystals were electron dense with transmission EM, consistent with their iron content (Fig. 3d). Stages of transformation of red cells from round to tetragonal were evident (Fig. 3d).

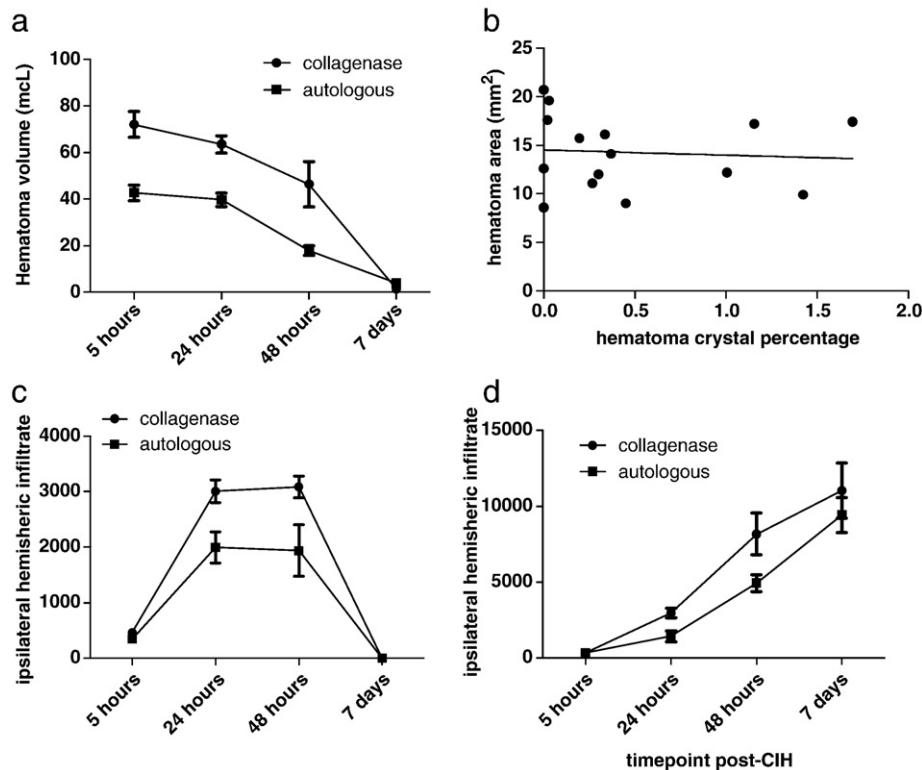


**Fig. 2 – Characterization of overall hematoma volumes and inflammatory infiltrate. (a)** Total hematoma volume was around 30% less in the autologous model (see text). There was a steeper decline in hematoma volume in this model, but in both models the hematoma had largely resorbed by 7 days. **(b)** There was no relationship between crystals percentage and hematoma area (cross-sectional through injection site) or volume (not shown) in 15 collagenase ICH brains at 24 h. **(c)** and **(d)** When adjusted for hematoma size, there was a greater leucocyte infiltrate in the autologous ICH group, which also peaked earlier. The time-course and extent of microglial infiltration/activation was similar in both models.

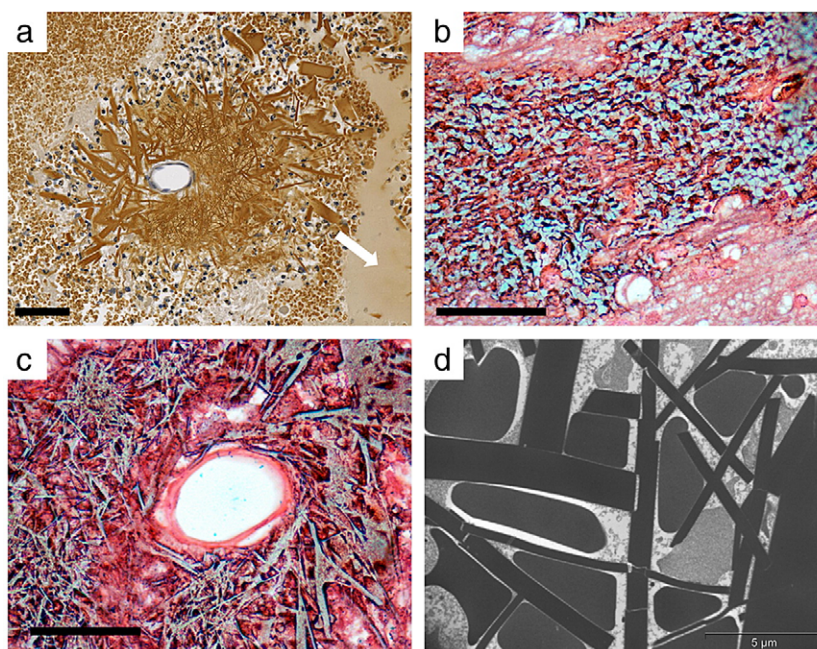


**Fig. 3 – Characterization of crystals in vivo using light and electron microscopy. Scale bar 100  $\mu\text{m}$  except EM (as shown). (a) DAB staining of section in Fig. 1a for hemoglobin. The perivascular crystal cluster demonstrated identical DAB staining to intact adjacent erythrocytes. Lysed hemoglobin (arrow) demonstrates fainter DAB reactivity; (b) and (c) Lillie's stain rat striatum, autologous ICH, 24 h. Similar blue staining was seen only in erythrocytes and crystals. (d) Transmission electron microscopy. Rounded erythrocytes evolving into tetragonal shapes.**

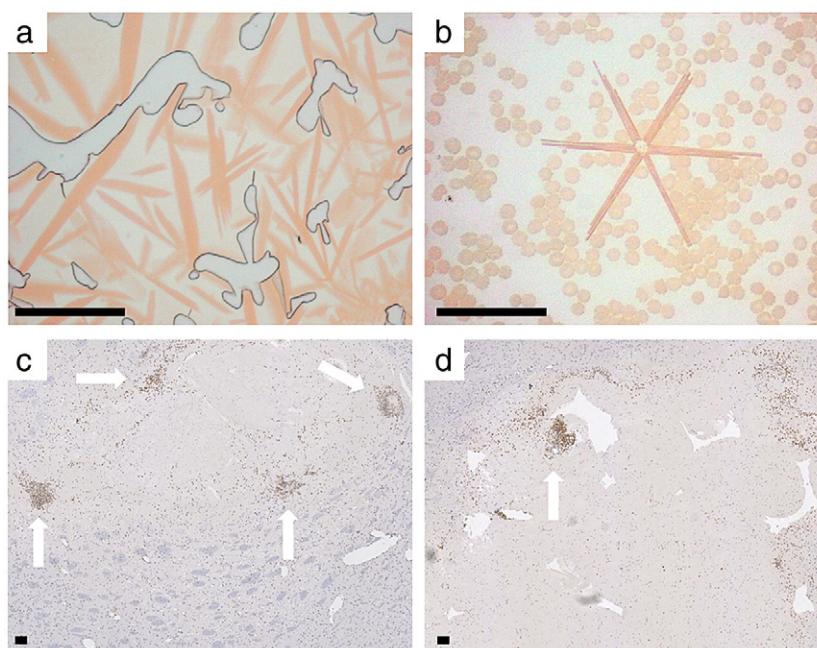


**Fig. 4 – Characterization of crystals in vitro with light microscopy and demonstration of neutrophil/crystal interactions. Scale bar 100  $\mu\text{m}$ . (a) Coverslipped rat whole blood direct microscopy 48 h. Areas of erythrocyte lysis adjacent to air bubbles becoming almost entirely occupied by hemoglobin crystals; (b) coverslipped rat whole blood direct microscopy 24 h. Complex 'snowflake' quaternary crystal structure. (c) Myeloperoxidase immunohistochemistry, rat striatum, autologous ICH, 24 h. Most of the neutrophil response to the ICH surrounds the four arrowed crystal clusters. (d) Myeloperoxidase immunohistochemistry, rat striatum, collagenase ICH, 24 h. Although the area of crystallization is easily identified by the surrounding neutrophils (arrow), both crystals and crystal-associated neutrophils make up a smaller proportion of the whole.**

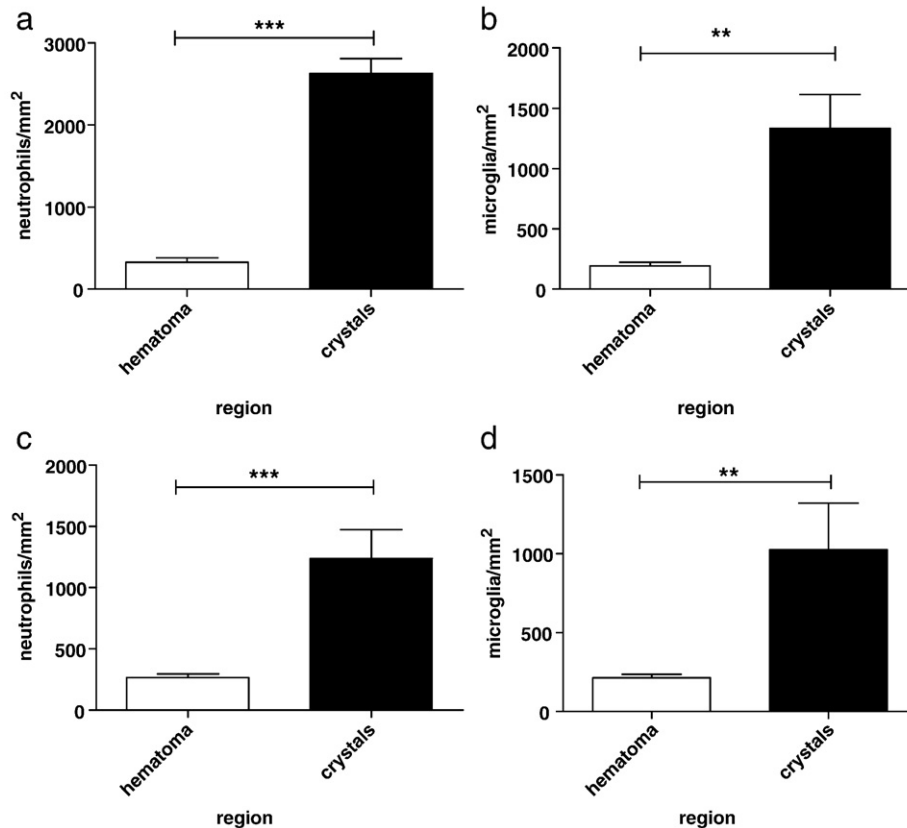


**Fig. 5 – Density of neutrophil and microglial infiltration around and within crystal clusters compared with that of the remaining hematoma, following autologous (a, b) and collagenase ICH (c, d). \*\*\* =  $p < 0.001$ , \*\* =  $p < 0.01$ .**

### 2.3. *In vitro* crystal formation

In the *in vitro* experiments, prominent clusters of crystals adjacent to fibrin thrombi were seen in 10/10 rats in the last 10  $\mu\text{L}$  (from 100  $\mu\text{L}$  total) of blood expelled directly from syringes onto glass coverslips. No crystals were seen initially in the first 10  $\mu\text{L}$  immediately after they were expelled or in heparinized blood (i.e. in fresh unclotted blood). However, at 6 h crystals could be identified in all smears, increasing in prominence, size and complexity over 24 to 48 h. Crystals were either needle-shaped or tetragonal and were most prominent in areas of hemolysis, especially around air pockets (Fig. 4a). In this location areas of erythrocyte lysis were observed to become entirely occupied by crystals (Fig. 4a). Occasionally complex quaternary structures were seen (Fig. 4b). No crystals were seen in ferret or human blood specimens (either clotted or unclotted) at any time point, suggesting that this propensity to crystallization is peculiar to rat blood.

### 2.4. Quantification of crystal-associated inflammatory cell infiltrate

At 5 h in both models a small number of perivascular and adherent intravascular neutrophils were evident, as well as small numbers within the clot itself. At 24 h, a dense rim of infiltrating neutrophils surrounded the hematoma in both models. Neutrophils were especially clustered around crystals (Figs. 1a–d, 4c, d). The neutrophilic infiltrate was significantly

denser among or within 50  $\mu\text{m}$  of crystals compared other areas (Figs. 5a, c;  $p < 0.001$ ). Likewise, in both models, a denser activated microglial response occurred around crystals than around the rest of the hematoma (Figs. 5b and d;  $p < 0.01$ ). The peri-crystalline neutrophilic infiltrate was denser in autologous ICH animals (Fig. 6a;  $p = 0.002$ ).

Although only occupying a small proportion of the hematoma volume, crystals were associated with a significant proportion of the inflammatory cell infiltrate, particularly neutrophils (Table 1). At lower magnification, areas of hemoglobin crystals could be identified by the surrounding dense cluster of neutrophils (Figs. 4c, d). In the autologous group at 24 h (the group which had the greatest hematoma crystal percentage) a greater percentage of hematoma crystallization was associated with a greater total neutrophilic infiltrate (Fig. 4c;  $p = 0.04$  for trend). At 48 h in both groups remnant areas of leucocytoclasia marked the sites of disintegrating crystals (Figs. 1c, d). No neutrophils were seen at 7 days (Fig. 2c). In both models neutrophil infiltrate peaked at 24–48 h, however in the autologous ICH animals an earlier peak was seen (Fig. 2c). The microglia response progressed over all timepoint studies, in a similar pattern in both models (Fig. 2d).

## 3. Discussion

Hemoglobin crystals can be derived *in vitro* from hemoglobin with varying degrees of difficulty, depending on the species of

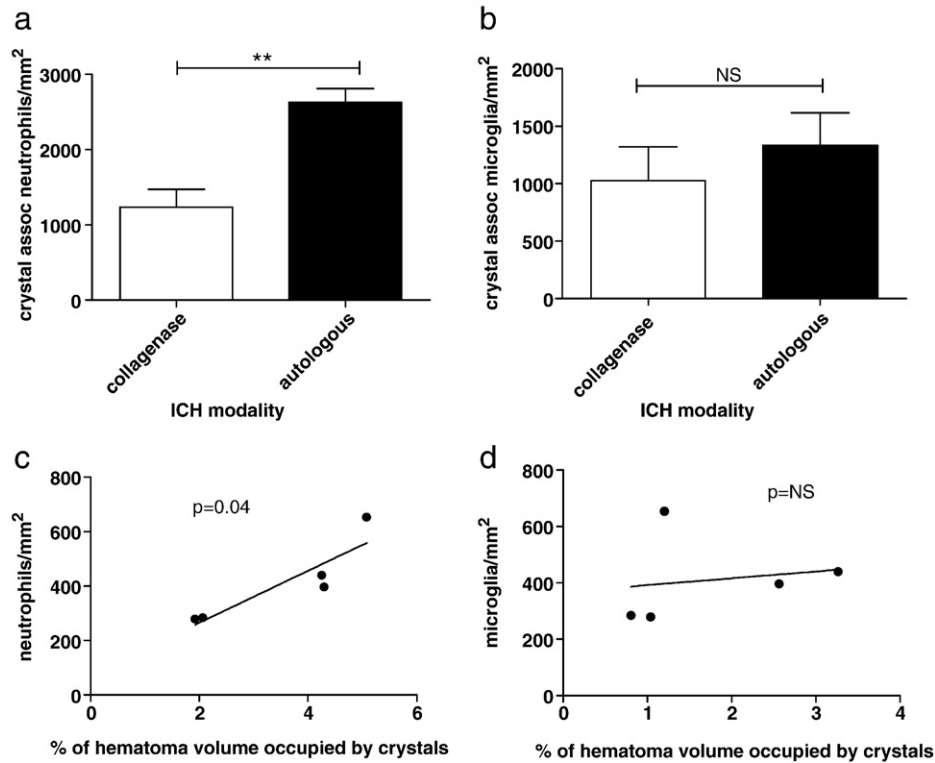


**Fig. 6 – (a, b) Comparison of the density of neutrophil (a) and microglial (b) infiltrate around crystals in the autologous and collagenase ICH models at 24 h. (c, d) Correlation of hematoma crystal percentage and hemispheric (injection site) neutrophil (c) and microglial (d) infiltrate following autologous ICH at 24 h. Cell counts are expressed per mm of injury (hematoma plus crystals), as the area of involvement at the injection site varied greatly between animals (Fig. 2b). \*\* =  $p < 0.01$ , NS = not significant.**

origin. Human hemoglobin is highly soluble and, *in vivo*, crystallization only occurs with structurally abnormal hemoglobin. *In vivo* crystallization of normal hemoglobin has been described in several species: rabbits (Simon and Burke, 1970) mice (Berman, 1967) and, most frequently, in the rat (Ghio et al., 2000; Harris and Chen, 1970; Madsen et al., 1982; Paakko et al., 1996; Rygh and Selvig, 1973; Salauze, 1993; Zachary et al., 2001). Rat hemoglobin has the poorest solubility (Boor, 1929) and readily forms crystals — perhaps existing in a partially crystalline state within erythrocytes (Brunori et al., 1982).

Hemoglobin crystallization in rats was first described following toxin-induced pulmonary hemorrhage (Harris and Chen, 1970) and has since been reported following pulmonary hemorrhage of varying etiologies (Ghio et al., 2000; Paakko et al., 1996; Zachary et al., 2001), as well as following graded pressure to rat dentition (Rygh and Selvig, 1973) and in the rat kidney after the injection of autologous blood (Madsen et al., 1982). It is of interest that, in the only previous study to systematically study the time-course of crystal appearance and resolution, that they appeared at 2 h, peaked at 24–48 h and were absent at 60 h, paralleling exactly our observations.

In the present study, crystals were shown to be hemoglobin crystals on the basis of their light and electron microscopic appearance, in particular, the lamellar inclusion bodies which are also present in erythrocytes, their endogenous peroxidase activity (indicative of a heme group), and the demonstration of ferrous iron within crystals (Fig. 3c). Furthermore, in the *in vitro* experiments (Fig. 4a), areas of

erythrocyte lysis became composed entirely of crystals when observed over time (hemoglobin comprises 98% of erythrocyte dry weight). Additionally, no crystals were demonstrated in blood from other species, and rat hemoglobin has a known propensity to crystallize. Although other blood-derived structures can under certain circumstance form crystals (hemin (Teichmann's crystals), ferritin and biliverdin), they were excluded by the features listed above.

Although others have commented on the concomitant presence of both hemoglobin crystals and inflammation (Harris and Chen, 1970; Madsen et al., 1982; Paakko et al., 1996), a direct pro-inflammatory effect of crystals has not previously been demonstrated. At 24 h all animals in the autologous blood injected group and most in the collagenase group demonstrated a dense peri-crystalline neutrophilic infiltrate, significantly more confluent than around or within areas of intact or lysed erythrocytes. Neutrophils tracked through areas of erythrocyte lysis to reach crystals, suggesting that crystals are strongly chemotactic, or more likely cause release of potent chemotactic factors. The identity of the cells responsible for this initial chemotactic factor release is not clear from this study; resident microglia and infiltrating leucocytes are likely candidates (Wang and Dore, 2007).

The pathways involved in crystal-evoked inflammation in the brain may mimic those activated in the periphery by *in vivo* crystallization of uric acid and calcium pyrophosphate dihydrate, which potentially evoke neutrophilic infiltration, resulting in acute arthritis (i.e. gout and pseudogout). The

pathways involved in these forms of crystal-induced inflammation are still under elucidation, however the Triggering Receptor Expressed on Myeloid cells 1 (TREM-1) and upregulation of the NALP-3 inflammasome are both implicated (Akahoshi et al., 2007; Martinon et al., 2006; Murakami et al., 2006). These pathways strongly upregulate IL-1 $\beta$ , (Murakami et al., 2006; Trendelenburg, 2008) which significantly enhances ischaemic stroke- and ICH-induced inflammation (Allan et al., 2005; Lu et al., 2006; Masada et al., 2001).

Inflammation after ICH in general, and the neutrophil response in particular, is on the whole detrimental (Wang and Dore, 2007). Although the sample size in this study was small, following autologous ICH, higher percentages of hemoglobin crystals in the hematoma 24 h after injury were correlated with a greater neutrophilic infiltrate (Fig. 6c), suggesting that hemoglobin crystal formation exaggerates the severity of inflammation. Up to 30% of neutrophils were associated with crystals in the autologous model at this timepoint, suggesting that the crystal-induced neutrophilic infiltrate may be severe enough to confound the assessment of inflammation in this model. In our experiments, the neutrophil peak infiltrate occurred earlier in the autologous model (Fig. 2c). Hemoglobin crystals may have been at least partly responsible. In the collagenase model, although crystals (per unit area) evoked similar inflammatory responses, as they comprised a smaller percentage of the hematoma overall (Table 1) they are less likely to affect the overall inflammatory response.

The onset of edema in autologous rat ICH is more rapid than in human ICH and red cells appear to be cleared more quickly (MacLellan et al., 2008; Xi et al., 2006). Hemoglobin crystals may contribute to this differential response. This concept could be proven by a comparison of inflammation after intracerebral injection of identical volumes of crystalline and non-crystalline rat hemoglobin, should such a preparation be feasible.

Hemoglobin crystals were more prominent in the autologous group at all timepoints, and were also immediately evident following the expulsion of clotted blood onto a coverslip, but not fresh or heparinized blood. When combined with the observation that collagenase ICH was complete at 5 h (indeed, largely complete at 2 h (MacLellan et al., 2008)) it is likely that the prominence of crystals in the autologous model is due to the infusion of clotted blood at pressure, rather than the timepoints selected for observation. Infusion of clotted blood through a small needle requires some force, and it is of interest that pressure in vivo promotes early (within 2 h) hemoglobin crystal formation (Rygh and Selvig, 1973), as opposed to spontaneous in vitro formation from blood at around 6 h. Whether pressure facilitates crystallization directly or by causing hemolysis is unclear. As the conformational structure (and hence crystal structure) of hemoglobin alters with oxygenation status, the tendency of crystals in the present study to cluster (in vivo) around blood vessels and form (in vitro) around air pockets suggests that it is oxy-, not deoxyhemoglobin, which crystallizes in this fashion.

Hemoglobin crystals were diminishing by 48 h and were absent at 7 days. How crystals break-down is not clear from this study. It is possible that a change in oxygenation status contributes to crystal dissolution, as the change from oxy- to deoxyhemoglobin (as assessed by MRI) occurs over a similar

time-course to crystal disappearance (i.e. progressively over the first 72 h (Bradley, 1993; MacLellan et al., 2008)). It is also possible that a direct effect of inflammatory cells (for instance hypochlorous acid from the neutrophilic respiratory burst) may facilitate crystal break-down.

Our study has several weaknesses. In particular, as this was a retrospective study on animals studied initially for other purposes, only sections through the hematoma centre were available for histological analysis. Assessment of whole brain hemoglobin crystal percentages and whole brain inflammatory responses were not possible, and whether our cross-sectional findings were therefore representative of the whole is uncertain. Additionally, for this previous study, the volumes of autologous blood and collagenase were chosen as they had been previously reported to cause similar final hematoma volumes (MacLellan et al., 2008). However, our autologous group had approximately a 30% smaller hematoma by visual (not spectrophotometric) assessment. Visual assessment overestimates collagenase hematoma volume (MacLellan et al., 2008) but it remains likely that our autologous ICHs were smaller; however, hematoma size did not appear to influence the degree of crystallization (Fig. 2b). Additionally, as specimens had been previously processed, we were unable to determine whether varied processing techniques may influence crystal formation or degradation. The absence of crystals at 5 h in the collagenase model strongly suggests, however, that crystal formation is arrested by perfuse fixation (crystals started to form in vitro from fresh blood at 6 h). Also, if crystal formation followed rather than preceded perfuse fixation, it would be difficult to explain why it preferentially occurred in regions of brisk leucocyte infiltration.

The degree of inflammation apparently evoked by crystal formation is probably only relevant to the autologous model (accounting for 22% vs of total neutrophil infiltrate vs 3% in the collagenase model). Our work adds to the known differences between the pathological responses to autologous and collagenase ICH (MacLellan et al., 2008). The presence of hemoglobin crystals in the autologous ICH model may theoretically be diminished by heparinization, or by using a larger bore needle and infusing blood more rapidly, to limit clotting and hemolysis. However, heparinization antagonizes thrombin, known to mediate secondary injury after ICH in multiple species (Hua et al., 2007). The second option would cause more needle trauma and intracerebral hematoma tracking. Autologous ICH in the mouse may be a further option, although hemoglobin crystallization has also been reported in this species, (Berman, 1967; Moore et al., 1964) (though less frequently).

Hemoglobin crystallization does not invalidate the rat autologous ICH model. It does, however, highlight methodological and species differences in ICH pathophysiology, and reiterates previous cautions regarding the extrapolation of results from rat to human ICH. The efficacy of potential treatments should be confirmed in other models and species before clinical translation.

---

#### 4. Experimental procedures

The University of Adelaide and Institute of Medical and Veterinary Science Animal Ethics Committees approved the

study, whose practices adhered to the Australian National Health and Medical Research Council code of practice for animal research.

#### 4.1. Intracerebral hemorrhage induction

The brains of 90 saline-injected ( $n=40$ ) collagenase ICH ( $n=30$ ) and autologous ICH ( $n=20$ ) Sprague–Dawley rats (weight 300–340 g) were examined retrospectively (weight 300–340 g); additionally, one animal of the same weight range was studied prospectively for electron microscopy (EM) 24 h after autologous ICH. Five animals were examined at each timepoint for each injury (5, 24, and 48 h and 7 days), plus an additional ten 24-hour-survival collagenase ICH animals.

Blood was also drawn from 10 Sprague–Dawley rats of the same weight range, 3 male ferrets and 3 male human volunteers.

Animals were anesthetized with isoflurane (5%) and placed in a stereotaxic frame (Kopf Instruments; “Tiowana”). Isoflurane was maintained at 1–2% in 30:70 mix of  $O_2:N_2$  at 1.4 L/min. Animals were placed on a thermostatically-controlled heating pad and rectal temperature was maintained at 36.5–37.5 °C. Autologous ICH animals were intubated and ventilated, with ventilator settings adjusted to keep parameters in the normal range (pH 7.4–7.5,  $CO_2$  35–45 mmHg,  $O_2$  100–150 mmHg). Collagenase ICH animals were placed on a nose cone.

In the autologous group, the femoral artery was cannulated and blood obtained for blood gas analysis. One hundred  $\mu$ L of blood was obtained from the femoral artery. A 0.7 mm burrhole was drilled in the rat skull (0.7 mm anterior, 3.0 mm lateral to bregma). Ten  $\mu$ L of blood was injected via a 26 G needle into the rat striatum (5.5 mm ventral relative to bregma). The needle was then advanced 0.5 mm, the injection paused (2 min) and the remainder (90  $\mu$ L) injected over 9 min. A matching volume of saline (100  $\mu$ L) was also injected into 20 rats using the same procedure. In the collagenase group 0.2 U of type VII bacterial collagenase (Sigma-Aldrich, Sydney, Australia) in 2  $\mu$ L normal saline or matching vehicle ( $n=20$ ) was infused in the same coordinates over 4 min via a 30 G needle. The needles were left in place for 5 min then withdrawn slowly. The burrholes were sealed with bonewax and wounds were closed with clips after irrigation with 0.5% bupivacaine.

Rats were placed two to a cage and fed and watered ad libitum. Rats were perfuse-fixed with 10% neutral buffered formalin 5, 24 and 48 h and 7 days post-infusion.

#### 4.2. Histological analysis

Brains were placed in a Kopf rodent blocker and sectioned into 2 mm slices. Sections were scanned immediately on a high-resolution (1200 pixels/inch) flatbed scanner. Hematoma volumes were calculated using Adobe Photoshop (v6.0.1, Adobe Systems Inc.) by manually outlining the hematoma area for the front and back of each 2 mm section, converting the pixel count into an area and multiplying the summed average by the slice thickness to give a volume for each slice; volumes were then summed for each rat.

Sections through the hematoma centre were stained with hematoxylin and eosin (H and E) and the immunoperoxidase method for neutrophils (1:60,000 polyclonal

anti-myeloperoxidase (Dako A0398, Sydney, Australia)) and activated microglia (mouse monoclonal anti-rat CD68 (AbD Serotec MCA341R, Oxford, United Kingdom)).

These sections through the hematoma centre were scanned (Nanozoomer, Hamamatsu, Hamamatsu City, Japan) and viewed with the associated proprietary viewing software (NDP view v1.1.27, Hamamatsu, Hamamatsu City, Japan). The area of both the total hematoma and the embedded crystals were manually delineated using the same software.

Neutrophils and activated microglia were counted on a single section for each rat for the entire ipsilateral hemisphere, the perihematomal region (within 50  $\mu$ m of hematoma) and the region around crystal clusters (within 50  $\mu$ m). Images were exported into ImageJ (v1.40g NIH, Bethesda, USA). Hematoxylin and diaminobenzidine stains were separated using color deconvolution (Ruifrok and Johnston, 2001) through an NIH ImageJ macro, following background subtraction with color correction. The deconvolved image was thresholded to remove background staining and ‘watershed’ function selected to separate touching cells. ‘Analyze particles’ was then selected, specifying particle size to ensure that only whole cells were counted. Manual counting was also performed on five sections to ensure the validity of this approach. To control for variation of hematoma size between models (Fig. 2a) inflammatory infiltrates were expressed per  $mm^2$  of injury on each slide (hematoma including crystals). For the 48 h and 7 day timepoints inflammatory infiltrates were expressed per  $mm^2$  of average injury at the 24 hour timepoint, as the hematoma area decreased progressively from 48 h onwards (Fig. 2a).

The intrinsic peroxidase activity of crystalline hemoglobin was demonstrated by the diaminobenzidine (DAB) method (Graham and Karnovsky, 1966). Lillie’s method was performed to demonstrate ferrous and/or ferric iron in red cells and crystals (Lillie and Geer, 1965) after heating to liberate iron from hemoglobin.

#### 4.3. Electron microscopy

Transmission EM was also performed on 1 autologous blood rat at 24 h post-ICH. Following perfuse fixation with 4% paraformaldehyde/2% glutaraldehyde in 0.1 M phosphate buffer, a 2 mm thick section from the hematoma centre was left overnight in EM fixative. This was rinsed in phosphate buffer, post-fixed in 1% osmium tetroxide, dehydrated and embedded in epoxy resin. 0.5  $\mu$ m thick survey sections were stained in toluidine blue and observed with a light microscope. 70–90 nm sections through areas containing hemoglobin crystals were collected onto grids and stained with uranyl acetate and lead citrate before being viewed with a Phillips CM100 transmission electron microscope.

#### 4.4. In vitro investigation of crystal formation

In complementary prospective in vitro experiments, 100  $\mu$ L of arterial blood was drawn from 10 rats and expelled at 10  $\mu$ L/min. Both the first and last 10  $\mu$ L were smeared on a glass slide, coverslipped and immediately inspected under direct microscopy for the presence of crystals. Three of 10 specimens were heparinized with 25 U porcine heparin. Specimens were taken from 3 ferrets and 3 humans and prepared identically (although

the human specimens were of venous blood). All specimens were also examined at 6, 24 and 48 h.

#### 4.5. Statistical analyses

Statistical analyses were performed with GraphPad Prism v 5.00 for Windows (GraphPad Software, San Diego, USA). Between-group comparisons were performed with two-sided unpaired t-tests with a 0.05 significance level. Linear regression analysis was performed to assess the correlation of hematoma crystal percentage with total inflammatory cell infiltrate and the correlation of hematoma size at 24 h in the collagenase group and percentage hematoma crystallization.

### Acknowledgments

This work was supported, in part, by the Neurosurgical Research Foundation, and by a Pfizer neurosciences research grant, as well as by a PhD scholarship for TJK from the National Health and Medical Research Foundation and the National Heart Foundation of Australia (Grant ID 465450).

### Appendix A. Supplementary data

Supplementary data associated with this article can be found, in the online version, at [doi:10.1016/j.brainres.2009.06.077](https://doi.org/10.1016/j.brainres.2009.06.077).

### REFERENCES

- Akahoshi, T., Murakami, Y., Kitasato, H., 2007. Recent advances in crystal-induced acute inflammation. *Curr. Opin. Rheumatol.* 19, 146–150.
- Allan, S.M., Tyrrell, P.J., Rothwell, N.J., 2005. Interleukin-1 and neuronal injury. *Nat. Rev. Immunol.* 5, 629–640.
- Berman, I., 1967. The ultrastructure of erythroblastic islands and reticular cells in mouse bone marrow. *J. Ultrastruct. Res.* 17, 291–313.
- Boor, A.K., 1929. A crystallographic study of pure carbonmonoxide hemoglobin. *J. Gen. Physiol.* 13, 307–316.
- Bradley Jr, W.G., 1993. MR appearance of hemorrhage in the brain. *Radiology* 189, 15–26.
- Brunori, M., Condo, S.G., Bellelli, A., Giardina, B., 1982. Hemoglobins from Wistar rat: crystallization of components and intraerythrocytic crystals. *Eur. J. Biochem.* 129, 459–463.
- Ghio, A.J., Richards, J.H., Crissman, K.M., Carter, J.D., 2000. Iron disequilibrium in the rat lung after instilled blood. *Chest* 118, 814–823.
- Harris, P.N., Chen, K.K., 1970. Development of hepatic tumors in rats following ingestion of *Senecio longilobus*. *Cancer Res.* 30, 2881–2886.
- Hua, Y., Keep, R.F., Hoff, J.T., Xi, G., 2007. Brain injury after intracerebral hemorrhage: the role of thrombin and iron. *Stroke* 38, 759–762.
- James, M.L., Warner, D.S., Laskowitz, D.T., 2008. Preclinical models of intracerebral hemorrhage: a translational perspective. *Neurocrit. Care* 9, 139–152.
- Lu, A., Tang, Y., Ran, R., Ardizzone, T.L., Wagner, K.R., Sharp, F.R., 2006. Brain genomics of intracerebral hemorrhage. *J. Cereb. Blood Flow Metab.* 26, 230–252.
- MacLellan, C.L., Silasi, G., Poon, C.C., Edmundson, C.L., Buist, R., Peeling, J., Colbourne, F., 2008. Intracerebral hemorrhage models in rat: comparing collagenase to blood infusion. *J. Cereb. Blood Flow Metab.* 28, 516–525.
- Madsen, K.M., Applegate, C.W., Tisher, C.C., 1982. Phagocytosis of erythrocytes by the proximal tubule of the rat kidney. *Cell Tissue Res.* 226, 363–374.
- Martinon, F., Petrilli, V., Mayor, A., Tardivel, A., Tschopp, J., 2006. Gout-associated uric acid crystals activate the NALP3 inflammasome. *Nature* 440, 237–241.
- Masada, T., Hua, Y., Xi, G., Yang, G.Y., Hoff, J.T., Keep, R.F., 2001. Attenuation of intracerebral hemorrhage and thrombin-induced brain edema by overexpression of interleukin-1 receptor antagonist. *J. Neurosurg.* 95, 680–686.
- Moore, R.D., Mumaw, V.R., Schoenberg, M.D., 1964. The structure of the spleen and its functional implications. *Exp. Mol. Pathol.* 33, 31–50.
- Murakami, Y., Akahoshi, T., Hayashi, I., Endo, H., Kawai, S., Inoue, M., Kondo, H., Kitasato, H., 2006. Induction of triggering receptor expressed on myeloid cells 1 in murine resident peritoneal macrophages by monosodium urate monohydrate crystals. *Arthritis Rheum.* 54, 455–462.
- Paakko, P., Anttila, S., Sormunen, R., Ala-Kokko, L., Peura, R., Ferrans, V.J., Ryhanen, L., 1996. Biochemical and morphological characterization of carbon tetrachloride-induced lung fibrosis in rats. *Arch. Toxicol.* 70, 540–552.
- Rosenberg, G.A., Mun-Bryce, S., Wesley, M., Kornfeld, M., 1990. Collagenase-induced intracerebral hemorrhage in rats. *Stroke* 21, 801–807.
- Ruifrok, A.C., Johnston, D.A., 2001. Quantification of histochemical staining by color deconvolution. *Anal. Quant. Cytol. Histol.* 23, 291–299.
- Rygh, P., Selvig, K.A., 1973. Erythrocyte crystallization in rat molar periodontium incident to tooth movement. *Scand. J. Dent. Res.* 81, 62–73.
- Salauze, D., 1993. Rat Haemoglobin Crystallisation? *Comp. Haematol. Int.* 4, 62.
- Simon, G.T., Burke, J.S., 1970. Electron microscopy of the spleen. 3. Erythro-leukophagocytosis. *Am. J. Pathol.* 58, 451–470.
- Squires, S., McFadzean, J.A., 1963. Behaviour of mammalian hemoglobin after freezing and thawing. *Nature* 199, 783–784.
- Trendelenburg, G., 2008. Acute neurodegeneration and the inflammasome: central processor for danger signals and the inflammatory response? *J. Cereb. Blood Flow Metab.* 28, 867–881.
- Wang, J., Dore, S., 2007. Inflammation after intracerebral hemorrhage. *J. Cereb. Blood Flow Metab.* 27, 894–908.
- Whisnant, J.P., Sayre, G.P., Millikan, C.H., 1963. Experimental intracerebral hematoma. *Arch. Neurol.* 9, 586–592.
- Xi, G., Keep, R.F., Hoff, J.T., 2006. Mechanisms of brain injury after intracerebral haemorrhage. *Lancet Neurol.* 5, 53–63.
- Zachary, J.F., Frizzell, L.A., Norrell, K.S., Blue, J.P., Miller, R.J., O'Brien, W.D., 2001. Temporal and spatial evaluation of lesion reparative responses following superthreshold exposure of rat lung to pulsed ultrasound. *Ultrasound Med. Biol.* 27, 829–839.